X-RAY SPECTROMETRY
X-Ray Spectrom. 2008; **37**: 608–614
Published online 24 September 2008 in Wiley InterScience
(www.interscience.wiley.com) DOI: 10.1002/xrs.1102

Determination of the composition of Ultra-thin Ni-Si films on Si: constrained modeling of electron probe microanalysis and x-ray reflectivity data

Tran M. Phung,[1] Jacob M. Jensen,[1] David C. Johnson,[1]* John J. Donovan[2] and Brian G. McBurnett[3]

[1] Department of Chemistry and Materials Science, University of Oregon, Eugene, OR 97403, USA
[2] Microanalytical Facility, CAMCOR, University of Oregon, Eugene, OR 97403, USA
[3] Department of Chemistry, University of the Incarnate Word, San Antonio, TX 78209, USA

Received 19 March 2008; Revised 24 June 2008; Accepted 3 July 2008

The homogeneous bulk assumption used in traditional electron probe microanalysis (EPMA) can be applied for thin-layered systems with individual layers as thick as 50 nm provided the penetration depth of the lowest accelerating voltage exceeds the total film thickness. Analysis of an NIST Ni-Cr thin film standard on Si using the homogeneous model yielded certified compositions and application of the same model to ultra-thin Ni-Si layers on GaAs yielded their expected compositions. In cases where the same element is present in multiple layers or in the substrate as well as the film, the homogeneous assumption in EPMA alone is not sufficient to determine composition. By combining x-ray reflectivity (XRR) thickness and critical angle data and using an iterative approach, quantitative compositional data in EPMA can be achieved. This technique was utilized to determine the composition of Ni-Si ultra-thin films grown on silicon. The Ni-Si composition determined using this multi-instrumental technique matched that of Ni-Si films simultaneously deposited on GaAs. Copyright © 2008 John Wiley & Sons, Ltd.

INTRODUCTION

Electron probe microanalysis (EPMA) has traditionally been used as a bulk analytical technique for the characterization of samples with a lateral spatial resolution of ~1 μm. Successful utilization of the technique requires an interplay between the heterogeneity of the sample, the beam energy, and the x-ray energies. Typical beam energies of 10–20 keV have excitation depths from 1–5 μm, lower beam energies (5–10 keV) have excitation depths of 0.1–1 μm, and ultra-low energies (below 5 keV) have excitation depths of 0.05–0.1 μm. However at such low energies, quantitative complexities arise due to fewer x-ray lines available, the low energy x-ray lines having a higher likelihood of absorption; the low over-voltage leads to lower efficiency of generated x-rays; possible substrate contamination and the excitation volume are sensitive to the absolute beam energy. Conventional EPMA often uses high-energy x-ray lines because they are easy to measure and are not strongly absorbed.[1] In layered systems, high-energy electrons are necessary to generate the emission of the high-energy photons, which are able to pass through the over-layers without being absorbed. In addition, the excitation depth generates x-rays further into the sample and therefore the x-rays must pass through more layers to get to the detector, creating an averaging or homogenizing effect. Complications arise, however, when trying to partition the distribution of x-rays from the various layers—particularly true when multiple layers contain the same element. This scenario is encountered frequently in a number of technologically important systems such as native oxide growth (TiO_2 on Ti) and epitaxial compound semiconductor ($Si_{1-x}Ge$ on Si).

Special procedures have been developed allowing for successful characterization of thin films, layered structures, and subsurface regions.[2–11] The data reduction models, e.g. the PAP model by Pouchou and Pichoir[12,13] or the Modified Surface centered Gaussian (MSG) model by Bastin and Heijliger,[14] are based on analytical expressions for the in-depth ionization distribution function, $\Phi(\rho z)$, which describes the intensity of the generated characteristic x-rays as a function of mass depth, (ρz). The penetration depth of x-ray generation in EPMA is approximated by (z_u):

$$z_u[\mu m] = (0.033/\rho)(E^{1.7}{}_o - E^{1.7}{}_c)(A/Z)$$

where E_o is the primary electron energy (accelerating voltage), E_c is the critical excitation energy of the x-ray line, ρ the density, A the atomic weight, and Z the atomic number of the material. Generally E_o is minimalized so that the maximum penetration depth of x-ray generation z_u is included entirely inside the film allowing it to be treated as a bulk sample. In comparison, the thin film scenario occurs when the film thickness is less than z_u. In this case, the x-ray intensities depend on the film composition, the film mass thickness (defined as the density times the thickness), the mean atomic number of the film, and the atomic number or composition of the substrate. For multielement films, the

*Correspondence to: David C. Johnson, Department of Chemistry and Materials Science, University of Oregon, Eugene, OR 97403, USA. E-mail: @oregon.uoregon.edu

ratio of the x-ray lines intensity for a single element (I_A) and the x-ray intensities of bulk standards (I_{std}) under the same conditions, known as the k-ratio, are plotted against multiple voltage measurements. STRATAGem and General Motors Research Film software (GMR) film modeling programs then iteratively fit the k-ratios with the mass thickness and composition as unknown parameters. Pouchou *et al*. successfully used low energy x-ray lines at low-accelerating voltages to analyze 80 nm Au films on 67 nm Au-Pd alloy (38% Pd) films on a W substrate and for a 435 nm B film with 5.3% Ti on 60 nm of TiB_2 on 1.25 μm of C on a SiC substrate.[4] Grazing-exit EPMA at multiple angles and accelerating voltages have also been successful at obtaining composition of various layers, but demand a level of expertise not accessible to the typical user and the grazing-exit geometry may not be applicable for all systems.[6,11,15,16]

In the work reported herein, we take an alternate approach to the problem of multiple layers containing the same element for the case of ultra-thin films by using both x-ray reflectivity (XRR) and EPMA in tandem. XRR is an accurate technique for the determination of film thickness[17] and the critical angle of the reflectivity scan can determine the density if the composition is known. EPMA, on the other hand, gives accurate compositional information if the thin film thickness and density are known.[1,18] Because total film thickness is precisely determined from XRR, it can be constrained in the modeling of the EPMA data, leaving two unknowns: composition and density. The two values can be determined by iteratively constraining either the mass thickness (i.e. density) value in EPMA or the composition in XRR until self-consistent parameters are obtained. A homogeneous model, a single layer with uniform composition, is adopted for EPMA analysis and the validity of this model is first verified with a National Institute of Standards and Technology (NIST) standard Cr-Ni multilayer thin film on Si. The iterative process for the redundant element scenario is then demonstrated with Ni-Si layers deposited simultaneously on silicon and GaAs substrates. The Ni-Si multilayer system is important for both technological and fundamental reasons. There are extensive applications for transition metal silicides as contact materials in integrated circuits, with the contacts typically prepared by a reaction between a thin transition metal film and silicon. Therefore, implementing a technique that enables the compositional analysis of metal silicides on silicon is important for technological reasons and the more general application of this approach has many significant scientific and technological applications.

EXPERIMENTAL

Standard reference material 2135c

The chromium and nickel Standard Reference Material (SRM) 2135c consists of nine alternating metal thin-film layers on a polished silicon (100) substrate; five of them are pure chromium and four are pure nickel, certified for total Cr and Ni thickness, single element layer-to-layer uniformity, Ni and Cr bilayer uniformity (periodicity), and single layer thickness. The individual layers have thicknesses that are ~57 nm for Cr and ~56 nm for Ni.[19–21] The total certified thickness and expanded uncertainties for the Cr and Ni layers as determined from x-ray fluorescence (XRF) spectroscopy and inductively coupled plasma (ICP) spectroscopy using a gravimetrically calibrated reference are 206.3 ± 13.8 μg/cm^2 and 197.4 ± 9.6 μg/cm^2, respectively.

Electron probe microanalysis (EPMA) was carried out at the University of Oregon's Cameca SX-50. Intensities of Ni Kα, Cr Kα, Si Kα, and O Kα lines were collected on separate wavelength dispersive spectrometers (WDS) using gas flow proportional detectors with P-10 gas. Data were collected at four different accelerating voltages (10, 15, 20, and 25 kV) with experimental intensities determined from the average of ten proximate positions on each sample. Ni, Cr, Si, and MgO were used as elemental standards. Raw intensities were corrected by procedures detailed by Armstrong.[22] Quantitative elemental analysis was determined by comparing experimental *k*-ratios to simulated values using STRATAGem thin film composition analysis software, which employs the PAP formalism developed by Pouchou and Pichoir.[12,13] The simulation employed a continuum correction for fluorescence, as well as a correction to account for approximately 20-nm thick carbon layer on the standards.

Ni-Si samples

Ni-Si multilayers were prepared by electron beam evaporation in a custom-built multisource deposition chamber operating at or below 1×10^{-6} torr. Ni rod (2.0 cm, 99.5 + %) and Si chips (1.0–2.5 cm, 99.9999 + %) were used as source materials. Alternate layers of Ni and Si were deposited with Ni always being deposited first. Films were deposited simultaneously onto Si(100) and GaAs(100) substrates roughly at 4 cm^2. In both cases, the native substrate oxide was left intact as a diffusion barrier.

XRR measurements were carried out on a Bruker D8 Discover Diffractometer. The incident beam was collimated with a 0.2-mm divergence slit and a parabolic multilayer mirror. The exit beam was conditioned with a 0.6-mm anti-scatter slit, a Soller slit assembly, and a 0.1-mm detector slit. When the intensity reached the detector exceeding 300 kcps, a 0.6-mm Cu attenuator was placed between the beam and the detector. Data was collected at 40 kV 40 mA. Thickness parameters were extracted from raw reflectivity curves using REFS Mercury reflectivity simulation software (Bede Scientific Ltd.).[23,24]

X-ray intensities of Ni Kα, Si Kα, and O Kα lines were collected under the same conditions as SRM 2135c for Ni-Si samples. The low energy Ni Lα was not examined because of a higher likelihood of absorption by the over-layers, complicated emission characteristics due to Coster-Kronig (non-radiative) transitions, and poorly determined mass absorption coefficients.[25,26] Owing to the high critical energy needed to excite the Ni Kα, accelerating voltages of 10, 15, and 20 kV were selected with Ni, Si, and MgO was used as elemental standards. Raw intensities were corrected and modeling was conducted using STRATAGem software.

DOI: 10.1002/xrs

X-RAY Spectrometry

BACKGROUND

X-ray reflectivity

Density measurement of a homogeneous thin film by XRR requires the determination of the critical angle θ_c.

The index of refraction n for x-rays of a material is given by:

$$n = 1 - \delta - i\beta \tag{1}$$

where δ is the anomalous dispersion correction, assuming the wavelength λ is far from the absorption edge and β related to the linear absorption coefficient μ. Both δ and β can be expressed in terms of the classical electron radius r_e, the electron density N_e, and the interaction wavelength λ as follows.

$$\delta = \frac{r_e N_e \lambda^2}{2\pi} \tag{2}$$

$$\beta = \frac{\mu\lambda}{4\pi} \tag{3}$$

Because δ is always positive, total external reflection occurs at the air/sample interface for all materials below a critical angle given by:

$$\theta_c \approx \sqrt{2\delta} \tag{4}$$

The critical angle is related to the average electron density N_e of the film, which in turn is related to the density of the total film. For the simplest argument of a bare substrate, the x-rays are reflected at angles less than the critical angle of the substrate. For SiO_2, this value is 0.42° 2θ. The three-system scenario of air/film/substrate results in fringes, called Kiessig fringes, due to constructive and destructive interferences of the reflected x-ray beam at the air/film interface and film/substrate interface. The position of the maxima θ_i of the specularly reflected x-ray beam is given by the Bragg relationship

$$m_i\lambda = 2d(\sin^2\theta_i - \sin^2\theta_c)^{1/2} \tag{5}$$

where m_i is the diffraction order of the i-th maxima, λ the wavelength of the incident x-ray (Cu Kα, 0.15418 nm), θ_i the angular position of the Bragg reflection, and θ_c the angular position of the critical angle. Absolute film thickness is determined by rearranging the equation—plotting the square of the sine of the maxima of the oscillations θ_i versus the square of the wavelength λ over two times the order m_i squared and extracting the thickness d from the slope, as given by the equation below.

$$\sin^2\theta_i = \left(\frac{\lambda}{2}\right)^2 \frac{m^2}{d^2} + \sin^2\theta_c \tag{6}$$

Therefore, the critical angle of the total film can be determined by the Kiessig fringes, the oscillations due to the total film thickness.[17] The critical angles for the samples as determined by the above relationship are seen in Table 3. The relationship between the critical angle θ_c and the density ρ of the total film is given by:

$$\rho = k\left(\frac{\sum_i x_i A_i}{\sum_i x_i Z_i}\right)\left(\frac{\theta_c}{\lambda}\right)^2 \tag{7}$$

where λ is the wavelength of the incident radiation, Z_i and A_i are the atomic number and mass number of component i, and x_i is the mole fraction of component i in the film.[17] The constant k is equal to π/r_0N_0 where r_0 is the classical electron radius and N_0 is Avogadro's number. Equation 7 suggests that the composition of the films—x_i—must be known in order to determine the density of the film (and therefore eventually the mass thickness). Because both the density and composition are related, a unique solution to one cannot be determined without knowledge of the other.

Proposed approach to the common element problem for ultra-thin films for EPMA

Problems to the application of EPMA to thin films arise particularly when the same element exists in multiple layers and a more complex iteration process is necessary. We propose a method to the problem of a common element in multiple layers and/or the substrate of ultra-thin films by constraining the modeling of the EPMA data. Pouchou showed that the mass thickness of the constituent layers of a pure Cu-Ni-Cu stack could be determined because the composition of each layer is effectively constrained to the bulk value.[4] Inversely, if the mass thickness could be constrained, the composition of the elements could be determined. Because XRR gives accurate film thickness and critical angle, only the density and composition are unknown. The film composition can be determined in EPMA by manually constraining the mass thickness to the known XRR thickness and an estimated density from the determined critical angle. Using an iterative approach, the composition determined by EPMA is then used to correct the initial density approximation until a self-consistent set of composition parameters is attained. A flowchart illustrating the iterative procedure developed to determine the composition of the layers is given in Fig. 1.

RESULTS AND DISCUSSION

Homogeneous model applications

Traditional EPMA assumes that the electron beam is exciting a homogeneous volume; therefore the matrix correction is being applied in a uniform manner, and there is one applicable $\phi(\rho z)$ profile for each element. In the case of an ultra-thin film with multiple layers, the same homogeneous assumption can be adopted. Instead of modeling the individual layers as distinct regions, the whole film is depicted as a single thin film of uniform composition. This model has been used for analysis of various compound, thin films and stratified layers, while the appropriate length scale for its use has been established by modeling the emitted intensities from the layers with various thicknesses. In the following, we probe the suitability of the homogeneous assumption at two length scales. First, it is used to determine the composition of thick layers of Cr and Ni approximately 50 nm each on a Si substrate. The same homogeneous bulk assumption is then applied to thinner Ni and Si layers (3.1 nm) on GaAs, given that as the film thickness approaches atomic scale the homogeneous assumption is increasingly valid.

DOI: 10.1002/xrs

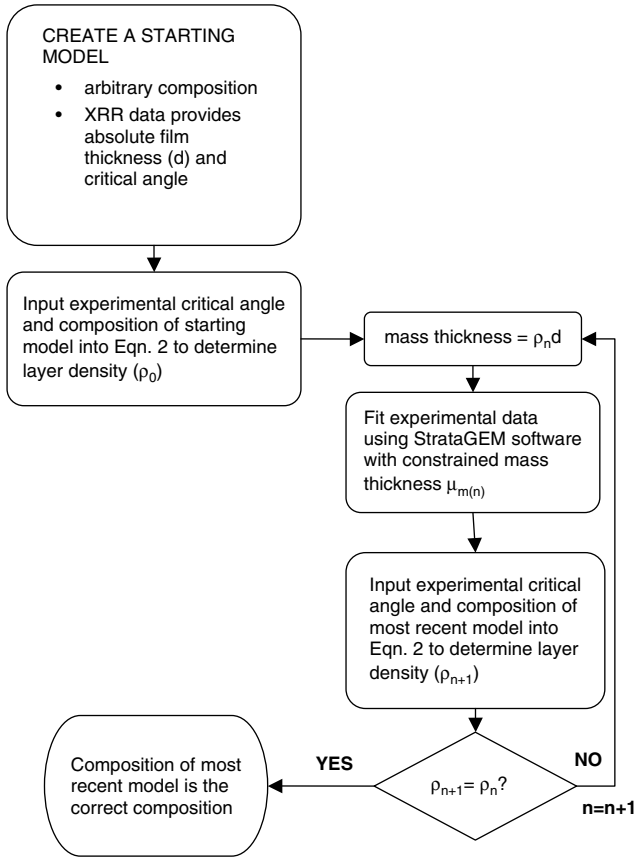

Figure 1. Flowchart for the extraction of composition parameters using EPMA and XRR from layered structures in which elements are simultaneously present in multiple layers.

Cr-Ni SRM 2135c standard

The sample consists of nine alternating layers of Cr (56 nm) and Ni (57 nm), with Cr as the top-most and bottom-most layer above the Si substrate. The sample was modeled as a homogeneous film of Ni and Cr on top of a Si substrate with the thickness and mass thickness values unconstrained. Oxygen was analyzed and the subsequent EPMA data was modeled to account for any metal oxide. The amount of oxygen was found to be below one atomic percent. The compositional results using the homogeneous model with accelerating voltages (15, 20, and 25 kV) that penetrate through to the substrate are a match to the experimental data (Fig. 2 and Table 1). In addition, the fit of the modeled k-ratio values past 15 kV mirror results for the system modeled as nine individual layers (Fig. 2). Therefore, the homogeneous model is a good approximation for the Cr and Ni film in the regime where the excitation volume includes the entire film and some of the substrate.

Table 1. Atomic ratio for SRM 2135c as determined from modeling as a homogeneous layer of Ni and Cr

Method	Cr	Ni	O
Certified	0.5110	0.4889	~
With 10 kV	0.4988	0.4716	0.0057
Without 10 kV	0.5084	0.4867	0.0049

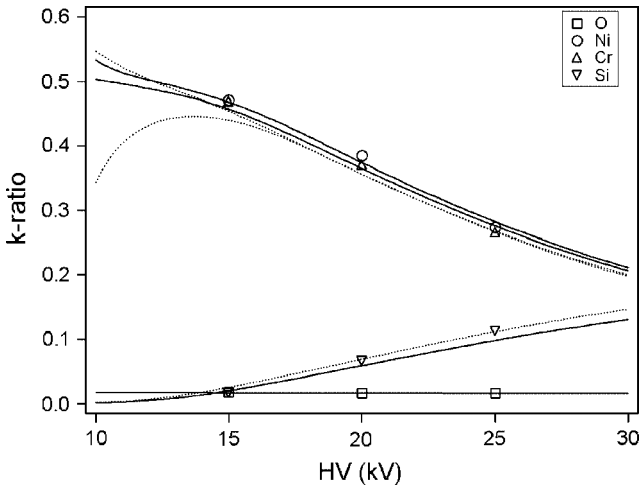

Figure 2. Comparison of experimental *k*-ratios (unfilled polygons) and calculated *k*-ratios for SRM 2135c as a function of accelerating voltage. Solid and dotted lines correspond to *k*-ratios representative of a homogeneous model and nine individual layers, respectively.

To show that it is necessary to use only accelerating voltages that penetrate through the entire film, intensity from a 10 kV beam was also acquired. At 10 kV, the electrons interact primarily with the top seven layers (Fig. 3). Results including the 10 kV accelerating voltage deviated from certified values with compositions for Ni, Cr, and Si never totaling above 97% (Table 1). The model was not able to account for the low experimental Ni k-ratio at 10 kV (Fig. 4). Therefore, *we conclude that the homogeneous bulk assumption works only when the excitation volume of the electron beam has sufficient energy to include both the layered film and substrate, creating a more averaged interaction volume.*

Ni-Si Samples on GaAs

The homogeneous assumption was also applied to thin layers of Ni and Si deposited on GaAs (samples 1A and 2A). Two samples consisting of 24 repeating units of Ni-Si were made. In the first sample, the deposition times for the Ni and Si layer were 14.1 and 63.7 sec, respectively, and in the second set, the deposition time for the Si was decreased to 24.7 sec while holding the Ni time constant at 14.1 sec. The samples were analyzed as deposited. XRR profiles of the samples show the evidence of layering, as seen by a single Bragg reflection arising from the compositional modulation (Fig. 5). The location of the Bragg reflection indicates that the bilayer thickness of the Ni and Si is 3.1 nm for sample 1A. The composition of the Ni-Si samples deposited on GaAs was determined by modeling the films as a homogeneous layer of Ni, Si, and O on a GaAs substrate (Table 2), again with the thickness and mass thickness unconstrained. The modeled k-ratios fit experimental data with the compositions converging to unity. As expected from the analysis of the Ni-Cr standard, the homogeneous assumption works for smaller length scales as well.

Iterative approach: Ni-Si samples on Si

Samples of Ni and Si on Si (1B and 2B) were simultaneously deposited with the GaAs samples described above. For

DOI: 10.1002/xrs

X-RAY Spectrometry

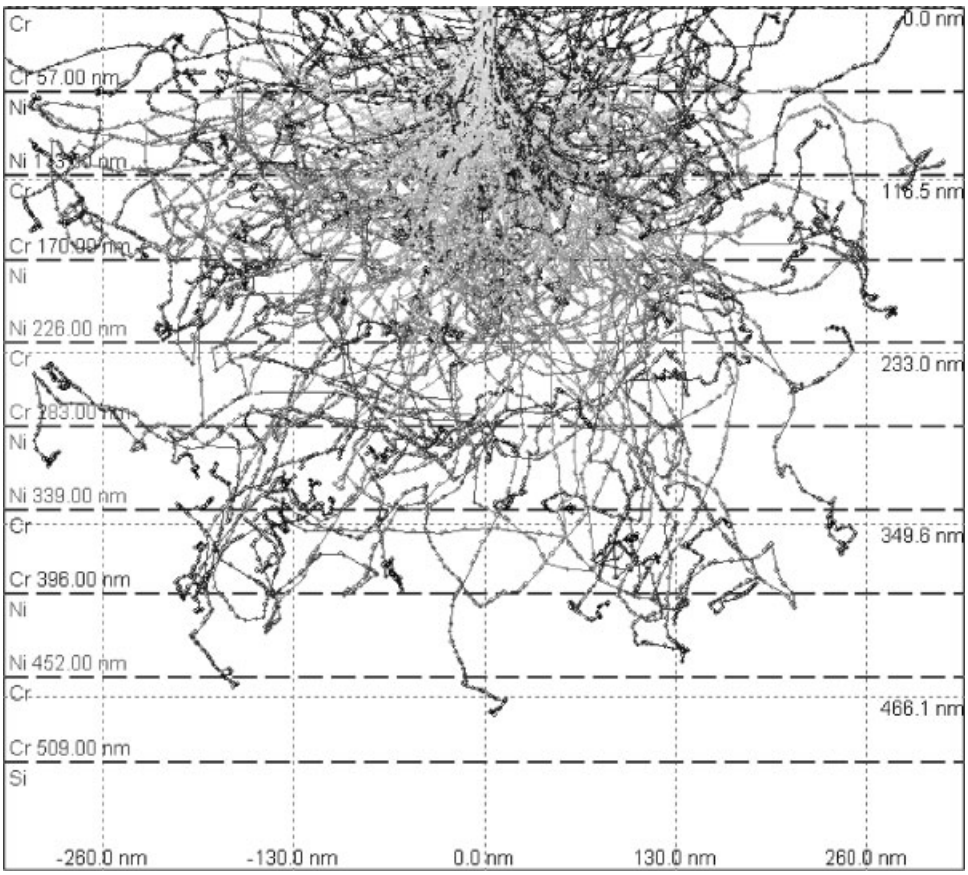

Figure 3. Penetration depth of 10 kV through SRM 2135c as modeled with Casino v2.42.

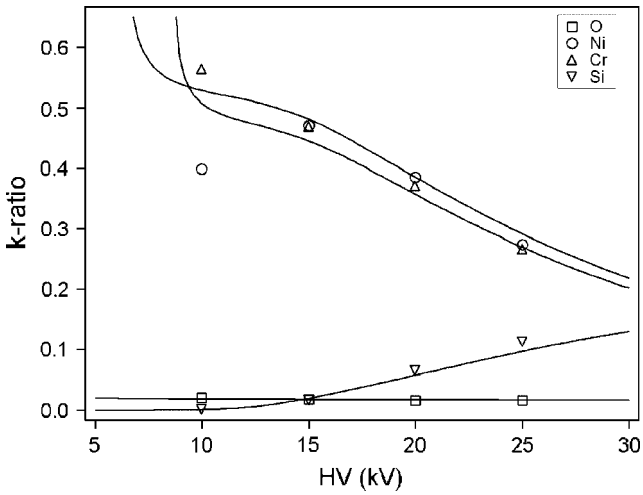

Figure 4. Comparison of experimental *k*-ratios (unfilled polygons) and calculated *k*-ratios (solid lines) for SRM 2135c as a function of accelerating voltage including 10 kV accelerating voltage.

compositional analysis with EPMA of the Si substrate samples, most of the Si x-ray signal originates from the substrate. Attempts to determine the composition of the Ni and Si layers on Si using the homogeneous assumption without any constraints on the mass thickness or thickness resulted in either divergence of the iterative scheme or convergence to physically unreasonable parameters (ultra-thin films of nearly pure nickel).

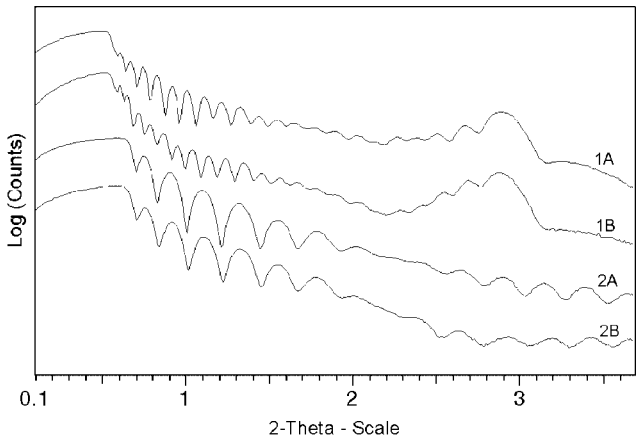

Figure 5. Raw x-ray reflectivity scans of Ni-Si samples.

Table 2. Normalized atomic fraction for nickel silicide samples as determined by EPMA. The composition of samples 1A and 2A (on GaAs) are determined by conventional thin film analysis methods. The composition of samples 1B and 2B (on Si) are determined by the iterative method described in the text

Sample ID	x(Ni)	x(Si)	x(O)
1A (GaAs)	0.25 ± 0.01	0.55 ± 0.02	0.21 ± 0.01
1B (Si)	0.27 ± 0.01	0.51 ± 0.02	0.21 ± 0.01
2A (GaAs)	0.45 ± 0.02	0.43 ± 0.02	0.12 ± 0.01
2B (Si)	0.43 ± 0.02	0.46 ± 0.02	0.11 ± 0.01

DOI: 10.1002/xrs

In order to determine composition, we apply the iterative procedure described in Fig. 1. The homogeneous assumption is used in the EPMA analysis with a constrained total film thickness from XRR data. XRR profiles of the Si samples show similar Bragg reflections and plots to determine the thickness and critical angle corroborate that the samples deposited on both GaAs and Si are identical within experimental error (Table 3). Figure 6 shows the resulting plots of the oscillation maxima extracted from Fig. 5 to determine the thickness and critical angle by means of Eqn. 6.

Below we illustrate the flow for the iterative process developed for the determination of the composition of layered films with common components with the substrate, using the specific case of sample 1B:

Starting Model: An arbitrary starting model of a homogeneous film with composition $Ni_{0.950}Si_{0.025}O_{0.025}$ is chosen. For the sake of illustration, the composition was intentionally made with much difference than the expected composition for the sample; in practice this is not necessary. Using Eqn. 7, the experimentally determined critical angle ($\theta_c = 0.276^\circ$), and the arbitrary starting composition, a layer density of $\rho_0 = 3.77\ g\ cm^{-3}$ is determined. Taken together with the experimentally determined absolute thickness, $d = 75.8$ nm, the mass thickness $\rho_0 d$ is calculated to be $28.6 \times 10^{-5}\ g\ cm^{-2}$.

ITERATION 1: With the mass thickness constrained to $28.6 \times 10^{-5}\ g\ cm^{-2}$, layer composition is determined using STRATAGem thin film software, producing the composition $Ni_{0.266}Si_{0.527}O_{0.207}$ for the homogeneous film. In order to fit the experimentally determined k-ratios, the software has shifted the composition from the initial Ni rich composition to being Si rich. The determined composition is then reapplied to Eqn. 7, using the experimentally determined critical angle of 0.276°, to give a layer density of $\rho_1 = 3.69\ g\ cm^{-3}$. The mass thickness is then recalculated using XRR thickness to be $28.0 \times 10^{-5}\ g\ cm^{-2}$.

ITERATION 2: With the mass thickness constrained to $28.0 \times 10^{-5}\ g\ cm^{-2}$, layer composition is determined using the thin film software package, producing the composition $Ni_{0.272}Si_{0.516}O_{0.212}$. Using Eqn. 7, the critical angle, and the composition produced by the thin film software, a layer density of $\rho_2 = 3.69\ g\ cm^{-3}$ is determined. Since $\rho_2 = \rho_1$, a self-consistent solution has been achieved. $Ni_{0.272}Si_{0.516}O_{0.212}$ is taken to be the composition of the Ni-Si layer for sample 1A. This result is obtained regardless of the initial value chosen for the starting composition.

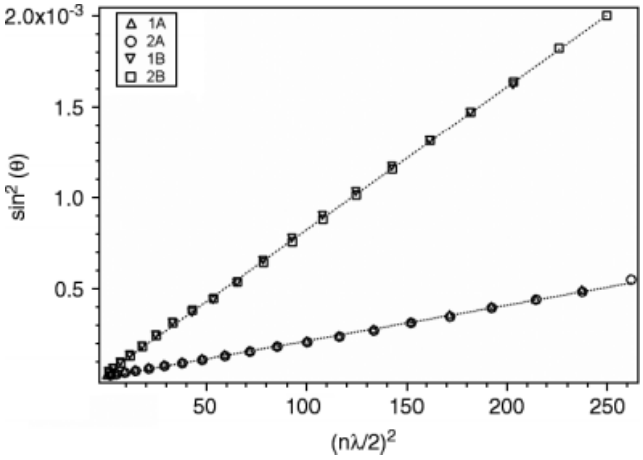

Figure 6. Plot of the oscillation maxima from Fig. 5 versus order for the Ni-Si samples.

Table 3. Thickness and critical angle parameters as determined by x-ray reflectivity

Sample ID	Substrate	Thickness (nm)	Critical angle (° θ)
1A	GaAs(100)	76 ± 3	$0.282 \pm 0.003^\circ$
1B	Si(100)	76 ± 2	$0.276 \pm 0.002^\circ$
2A	GaAs(100)	34.9 ± 0.6	$0.333 \pm 0.002^\circ$
2B	Si(100)	35.5 ± 0.9	$0.331 \pm 0.002^\circ$

The method detailed above was also used to determine the composition of 2B. In both cases, the compositions for the films deposited on Si match their GaAs grown counterparts to within experimental error. Furthermore, the difference in composition between the two sets is qualitatively consistent with the deposition parameters. In both cases, arbitrary starting compositions were able to converge to the *true* composition within a few iterations. The tabulated results for all Ni-Si samples are given in Table 2. To ensure goodness of fit, the experimental k-ratios were compared with calculated k-ratios determined by STRATAGem and GMR films.[27] The comparison between the experimental and calculated data for the Ni-Si layers on Si for the two samples is illustrated in Fig. 7. By constraining the film thickness to a value determined by XRR, the homogeneous model was able to determine the composition of the Ni-Si films on Si.

As with most buried geometry EPMA systems, modifications to the procedure may be necessary or advantageous depending on the system under investigation. The parameters must depend on the mass thickness of the buried layer in addition to the adsorption characteristics of the emitted

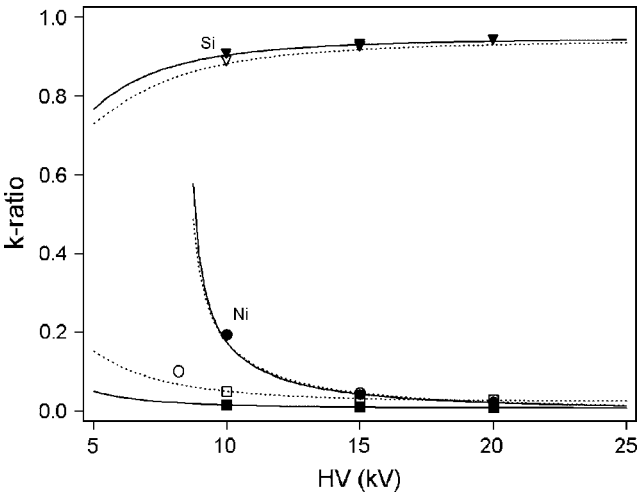

Figure 7. Comparison of experimental *k*-ratios and calculated *k*-ratios for sample 2A (filled polygons, solid lines) and 2B (unfilled polygons, dotted lines) on Si using homogeneous model coupled with XRR data as a function of accelerating voltage.

DOI: 10.1002/xrs

X-RAY Spectrometry

radiation in the upper layers. For example, the composition-dependent portion of Eqn 7, $\sum_i x_i Z_i \Big/ \sum_i x_i A_i$ is effectively constant when the film under investigation is composed entirely of light elements (i.e., $Si_{1-x}C_x$), in that $Z/A \approx 2$ for elements B through Ca. Thus, the film density is effectively independent of composition. In such scenarios the film density may be determined directly from the critical angle, enabling unique determination of the mass density without the iterative procedure. In most cases the composition dependence of the critical angle–density relationship is weak and the iterative method should work well. In the $Ni_{1-x}Si_x$ system investigated herein, the total variation in $\sum_i x_i Z_i \Big/ \sum_i x_i A_i$ is less than 5% over the range $0 < \times < 1.0$.

It should be noted that the characterization of layer densities in multilayer stacks sometimes requires more information than just the critical angle, in that the critical angle may correspond to the density of the top layer only or the average density of the total stack; multiple critical angles may sometimes exist, particularly when films of less density material overlay a much denser film. Users should be careful while using the critical angle for more complicated systems as it may lead to erroneous results and should rely on simulations of the XRR data to arrive at a density value for the layer whose composition is to be determined.

CONCLUSION

While the homogeneous model is used to determine composition in traditional EPMA, it can also be used for layered films with individual layers as thick as 50 nm, as demonstrated with the Ni-Cr standard. However, the caveat is that electron energies used in the analysis must penetrate through the entire film of interest to the underlying substrate in order that the emitted x-rays are subjected to the averaged absorption effects of the entire structure. We were able to use the same approach to determine the composition of thin Ni-Si layers on GaAs. In instances with common components in the film and substrate, the homogeneous model in EPMA analysis must be coupled with XRR thickness and critical angle data in an iterative procedure to successfully determine the composition of the film. This was successfully demonstrated with Ni-Si layers deposited on Si without using low energy lines or low-accelerating voltages. Simultaneous analysis using XRR and EPMA overcomes the key limitations inherent in each individual technique. XRR provides accurate determination of thickness and critical angle. Density can be determined by the critical angle provided the composition of the sample is known. The strength of EPMA is accurate characterization of composition, provided the model is representative of the experimental data. Using both techniques in tandem draws on the strengths of each technique to arrive at a robust, self-consistent solution.

Acknowledgements

Initial funding for this work was provided by NSF (DMR-9813726). Ongoing support for this project was funded from research monies associated with an NSF (DMR-0103409) and IGERT fellowships (DGE-0114419) for T.M. Phung and J.M. Jensen.

REFERENCES

1. Heinrich KFJ. *J. Phys. Colloq.* 1984; **45**(C2): 3.
2. Pouchou JL, Pichoir F. *Scanning Microsc. Suppl.* 1993; **7**: 167.
3. Pouchou J-L. *Anal. Chim. Acta* 1993; **283**(1): 81.
4. Pouchou J-L. *Mikrochim. Acta* 2002; **138**(3–4): 133.
5. Spolnik Z, Tsuji K, Saito K, Asami K, Wagatsuma K. *X-ray Spectrom.* 2002; **31**(2): 178.
6. Spolnik Z, Zhang J, Wagatsuma K, Tsuji K. *Anal. Chim. Acta* 2002; **455**(2): 245.
7. Tsuji K, Saito K, Asami K, Wagatsuma K, Delalieux F, Spolnik Z. *Spectrochim. Acta, Part B: Atom. Spectrosc.* 2002; **57B**(5): 897.
8. Tsuji K, Spolnik Z, Wagatsuma K, Saito K, Asami K. *Mater. Trans.* 2002; **43**(3): 414.
9. Willich P. *Mikrochim. Acta, Suppl.* 1992; **12**: 1.
10. Campos CS, Coleoni E, Trincavelli J, Kaschny J, Hubbler R, Soares MRF, Vasconcellos MAZ. *X-ray Spectrom.* 2001; **30**(4): 253.
11. Awane T, Kimura T, Suzuki J, Nishida K, Ishikawa N, Tanuma S. *Anal. Chem.* 2003; **75**(15): 3831.
12. Pouchou JL, Pichoir F. *Microbeam Analysis* (20th edn) San Francisco Press: San Francisco, CA, 1985; 104.
13. Pouchou JL, Pichoir FMA. *Microbeam Analysis* (23rd edn) San Francisco Press: San Francisco, CA, 1988; 315.
14. Bastin GF, Dijkstra JM, Heijligers HJM. *X-ray Spectrom.* 1998; **27**(1): 3.
15. Spolnik Z, Tsuji K, Van Grieken R. *X-ray Spectrom.* 2004; **33**(1): 16.
16. Tsuji K, Spolnik Z, Wagatsuma K, Nagata S, Satoh I. *Anal. Sci.* 2001; **17**(1): 145.
17. Holy V, Pietsch U, Baumbach T. *High Resolution X-ray Scattering from Thin FIlms and Multilayers*. Springer-Verlag: Berlin, 1999.
18. Duncumb P. *J. Anal. Atom. Spectrom.* 1999; **14**(3): 357.
19. Fine J, Navinsek B. *J. Vac. Sci. Technol.* 1985; **A3**: 1408.
20. Fine J, Lindfors PA, Gorman ME, Gerlach RL, Navinsek B, Mitchell DF, Chambers GP. *J. Vac. Sci. Technol.* 1985; **A3**: 1413.
21. Fine J, Navinsek B. *Surf. Interface Anal.* 1988; **11**: 542.
22. Armstrong JT. *Microbeam Anal.* (23rd edn). San Francisco Press: San Francisco, 1988; 239.
23. Wormington M, Panaccione C, Matney KM, Bowen KD. *Philos. Trans. R. Soc. London, Ser. A: Math. Phys. Eng. Sci.* 1999; **357**(1761): 2827.
24. Wormington M, Bowen DK, Tanner BK. *Mater. Res. Soc. Symp. Proc.* 1992; **238**: 119.
25. Labar JL. *Microbeam Analysis* (23rd edn) San Francisco Press: San Francisco, CA, 1988; 253.
26. Labar JL, Salter CJ. *Electron. Probe Quant.* edited by KFJ Henrich, DE Newbury. Plenum Press: New York, 1991; 223.
27. Waldo R. *Microbeam Anal.* (23rd edn). San Francisco Press: San Francisco, 1988; 310.